Electronic supplementary information for The role of shape disorder in the collective behaviour of aligned fibrous matter

S. Salamone[1], N. Schulmann[1], O. Benzerara[1], H. Meyer[1], T. Charitat[1]*, C. M. Marques[1]

[1]UPR 22/CNRS, Institut Charles Sadron, Université de Strasbourg,
23 rue du Loess, BP 84047 67034 Strasbourg Cedex 2, France

November 26, 2018

Contents

S1 Single fiber characterisation

S1.1 Eigenfunctions of the square Laplacian operator

In what follow, It is convenient to decompose fiber shape in the basis of the eigenfunctions $\Phi_{q_i}(x)$ of the square Laplacian operator ($\left(\partial^2/\partial x^4 - q^4\right)\Phi_q(x) = 0$) associated to curvature elasticity [1, 2].

$$\zeta_0(x) = \sum_i \zeta_{0,q_i}\Phi_{q_i}(x). \tag{S1}$$

*Address for correspondence, thierry.charitat@ics-cnrs.unsitra.fr

Choosing boundary conditions ensuring that there are no forces nor torques on the strands we have

$$\Phi_{q_i}(x) = \frac{\cosh(\alpha_i) - \cos(\alpha_i)}{\sinh(\alpha_i) - \sin(\alpha_i)} \left[\sinh\left(q_i x\right) + \sin\left(q_i x\right)\right] - \left[\cosh\left(q_i x\right) + \cos\left(q_i x\right)\right] \ , \tag{S2}$$

where the numerical coefficients $q_i L_0$ are determined from the relation $\cos\left(q_i L_0\right)\cosh\left(q_i L_0\right) = 1$. The solutions obey approximately $q_i = \left(i + 1/2\right)\pi/Na$ where $i \in \mathbb{N}^\star$. The wave vectors q_i were picked uniformly with $i = i_{min}...N$.

S1.2 Experimental fibers

S1.2.1 Individual fiber properties

An example of each type of fiber is given in Fig. S1. PP1 fibers appear to be highly disordered while PP2 fibers exhibit a dominant mode of wavelength 5 mm together with a distribution of wavelengths of smaller amplitudes. DEN fibers are more or less crenellated.

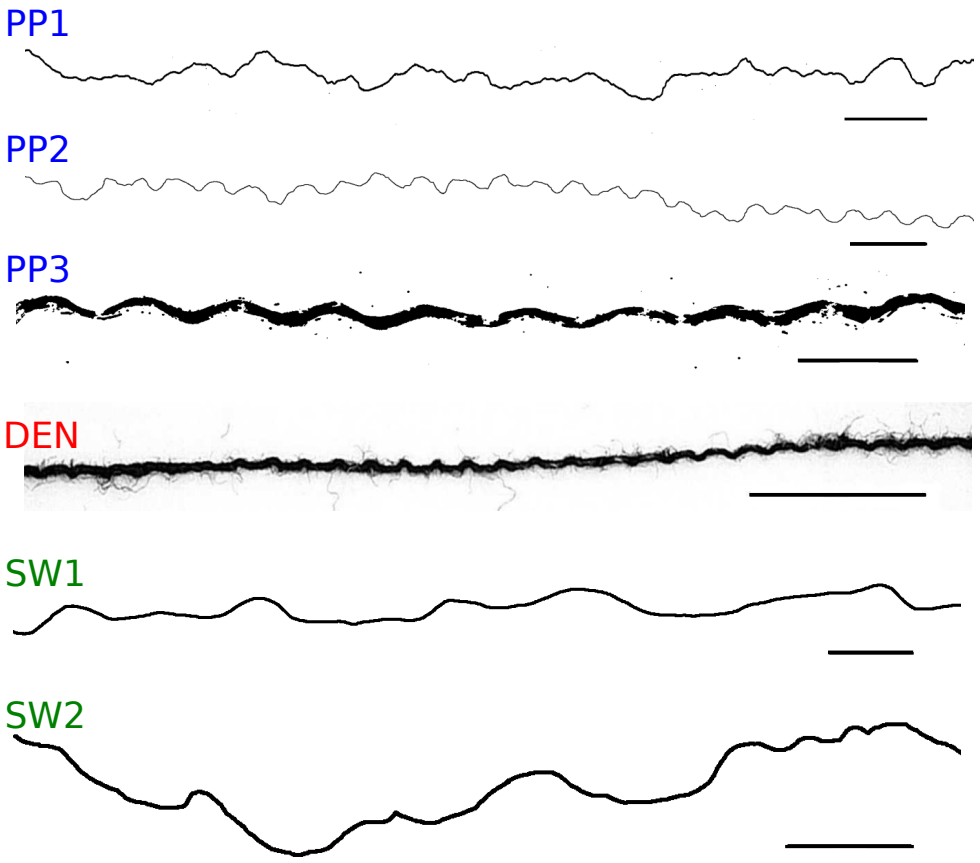

Figure S1: Individual images of all types of fibers studied: from top to bottom PP1, PP2, PP3, DEN, SW1 and SW2. Bar corresponds to 1cm.

Transversal section diameters are of the order of 20 - 100 μm for PP fibers, 500 μm for DEN fibers and 200-300 μm for SW1 and SW2.

S1.2.2 Individual fiber shapes

Fiber shapes are characterised as follow. We first performed images of many fibers (~ 50 per samples) using a scaner. We then extract the coordinate of fiber images to obtain the function $\zeta_0(x_i)$ that we expand numerically on the $\Phi_{q_i}(x)$ basis as eqn S1.

To check our method we have performed a test experiment as follow. We first impose an initial normal distribution of modes of variance $\zeta_{0,q}^{(\mathrm{ini})}$ given by

$$\langle \zeta_{0,q}^2 \rangle = \frac{c(\alpha)}{q^\alpha}, \tag{S3}$$

and corresponding to a Power Law Disorder (PLD). We choose randomly amplitudes $\zeta_{0,q}^{\mathrm{ini}}$ following this normal distribution in order to plot a test fiber $\zeta_0^{(\mathrm{ini})}(x)$ (see Fig.). We then printed and scanned this image as for experimental case (see Fig. S2(a)). We use the ImageJ software to extract the coordinates of the points which allows us to get $\zeta_0^{(\mathrm{num})}(x)$ (see Fig. S2). We then apply our transform analysis procedure and obtain the measured mode distribution $\zeta_{0,q}^{(\mathrm{mes})}$ (Fig. S2(d)):

$$\zeta_{0,q}^{(\mathrm{ini})} \longrightarrow \zeta_0^{(\mathrm{ini})}(x) \longrightarrow \zeta_0^{(\mathrm{num})}(x) \longrightarrow \zeta_{0,q}^{(\mathrm{mes})}. \tag{S4}$$

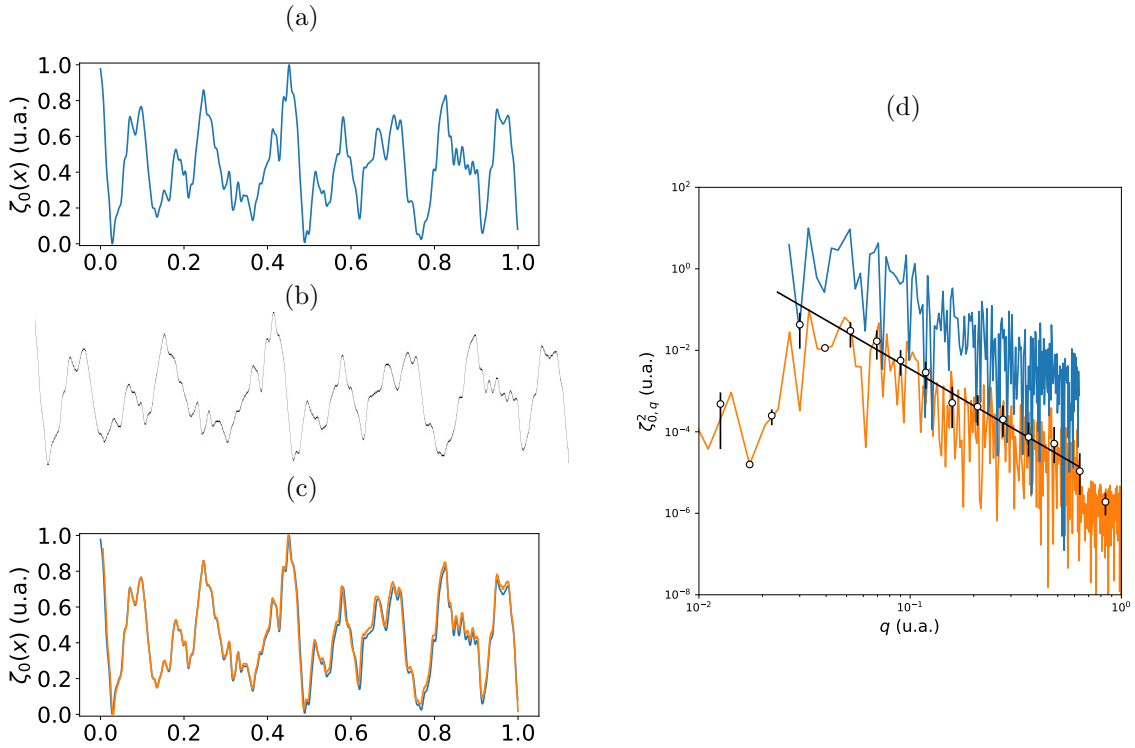

Figure S2: (a) Initial fiber $\zeta_0^{(\mathrm{ini})}(x)$ generated from a random spectra $\zeta_{0,q_i}^{(\mathrm{ini})}$. (b) Printed and digitized fiber $\zeta_0^{(\mathrm{num})}(x)$. (c) Comparison between (a) and (b). (d) Initial spectra $\zeta_{0,q_i}^{(\mathrm{ini})}$ (▬) and numerical spectra $\zeta_{0,q}^{(\mathrm{mes})}$ obtained using our method. The amplitudes are shifted for sake of clarity. (○) corresponds to moving average and (▬) to initial power law.

Results are plotted on Fig. S2(d), where we compare the initial mode distribution $\zeta_{0,q}^{\mathrm{ini}}$, the calculated one $\zeta_{0,q}^{(\mathrm{mes})}$ and the initial power law distribution. It clearly demonstrate the validity of our method.

We present in Fig. S3(a) and (b) an example of shape analysis for PP1 fibers. Fig. S3(a) shows the spectra obtained for 4 different fibers. We also verify by simple visual observation that all the fibers of a stack are similar. Fig. S3(b) shows the comparison between the spectrum obtained for a fiber and that obtained by averaging over 40 fibers.

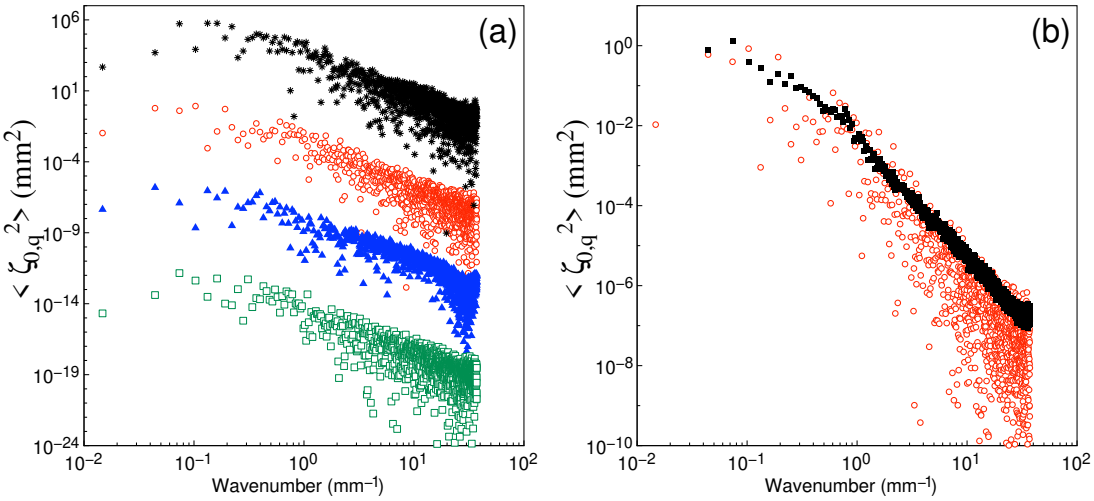

Figure S3: Shape analysis for PP1 samples: (a) $\zeta_{0,q}^2$ for 4 different PP1 fibers and (b) average spectra $\langle \zeta_{0,q}^2 \rangle$ over 40 fibers.

S1.2.3 Videos of individual fiber bending modulus measurements

As described in the main paper, fiber bending modulus was measured by measuring oscillations of single fiber for SW1 and SW2 samples. A video showing an example of these experiments is shown as ESI (oscillation-FE1(fps25).avi).

For PP and DEN samples, we have developped a stretching method also described in paper. A video showing an example of these experiments is shown as ESI (etirement(fps25).avi).

S1.3 Numerical fibers

We build the shapes of the isolated fibers from a given mathematical function $\zeta_0(x)$ along which we place N monomers sequentially, at the equilibrium distance, $a = 1$, of the monomer-monomer bond interactions, setting at the same time the corresponding equilibrium angles $\theta_{0,i}$. At the end of this process, we have a fiber of N monomers in an equilibrium shape close to the prescribed function $\zeta_0(x)$. In the following, we will consider three different cases for $\zeta_0(x)$. $L_0 = Na$ is the real length of the fiber, and L its projection on the x-axis.

S1.3.1 Perfectly ordered Reference state (Ref)

We first consider fiber stacks of sinusoidal strands:

$$\zeta_0^{(i)}(x) = d_0/2 \cos(2\pi x/\lambda_i + \varphi_i) \tag{S5}$$

where λ_i and φ_i are respectively the ith fiber's wavelength and the relative phase position.

In order to calibrate our simulation method against predictions from continuous elasticity theory, we test simple systems corresponding to single fibers with sinusoidal shapes, confined between parallel walls.

In practice, for consistency with the more complicated systems where periodic boundary conditions are imposed, instead of simulating single chains between walls we simulate periodic systems consisting of pairs of chains with identical sinusoidal shapes and opposite phases

$$\forall i,\ \begin{cases} \lambda_i = \lambda \\ \varphi_i = (1-(-1)^i)\frac{\pi}{2} \end{cases} . \tag{S6}$$

The opposite phases coupled with chains small roughness due to the shapes of individual monomers insure that chains do not slide. In the following we will refer to this system as the *reference state* (Ref).

S1.3.2 Disordered states

i. Single mode disordered systems (SMD) We consider a first class of disorder by adding a random translation phase shift φ_i homogeneously distributed in phase space $\varphi_i \in [0, 2\pi]$ in equation S5. A small dispersion of wavelengths is also introduced (λ_i are chosen from a Gaussian distribution of mean value λ_0 and variance $\delta\lambda$) to avoid perfect stacking of fibers :

$$\varphi_i \in [0, 2\pi], \tag{S7}$$

$$\mathcal{P}(\lambda_i) = \frac{1}{\sqrt{2\pi\sigma^2}} e^{-\frac{(\lambda_i-\lambda_0)^2}{2\delta\lambda^2}} . \tag{S8}$$

ii. Power-law disordered systems (PLD) For *power-law disorder*, fiber shapes were obtained by constructing $\zeta_0(x)$ as a superposition of the eigenfunctions with amplitude ζ_{0,q_i} :

$$\langle \zeta_{0,q_i}^2 \rangle = \langle \zeta_0^2 \rangle \left(\frac{\pi}{L q_i}\right)^{\alpha} \zeta\left(\alpha, i_{min} + 3/2\right)^{-1}, \tag{S9}$$

where $\zeta(\alpha, i_{min} + 3/2)$ is the generalized zeta function [3]:

$$\zeta(\alpha, a) = \sum_{i=0}^{+\infty} \frac{1}{(a+i)^{\alpha}}. \tag{S10}$$

We removed the largest wavelength mode $q \leq q_{i_{min}}$ to avoid fiber regular packing (we test $i_{min} = 1$ to 7) and choose to focus on systems with power-law distributions of wavelengths with associated amplitudes

We use values of the root-mean-square amplitude $\zeta_0 = \sqrt{\langle \zeta_0^2 \rangle}$ of a fiber in the continuous distribution model as a way of monitoring the vertical average extension of the fibers. $\langle \zeta_0^2 \rangle$ is given by :

$$\langle \zeta_0^2 \rangle = \frac{1}{L} \int_0^L \mathrm{d}x\ \zeta_0(x)^2, \tag{S11}$$

where L is the projected length of the fiber.

In order to check the consistency between analytical and numerical descriptions, a family of shapes of the type $\langle \zeta_{0,q_i}^2 \rangle = C/q_i^{\alpha}$ was generated and then the relation

$$\frac{\langle \zeta_0^2 \rangle}{C} = \zeta\left(\alpha, i_{min} + 3/2\right) \left(\frac{L}{\pi}\right)^{\alpha}. \tag{S12}$$

was plotted, see Fig. S4, with $\langle \zeta_0^2 \rangle$ measured by the smallest eigenvalue of the fiber gyration tensor.

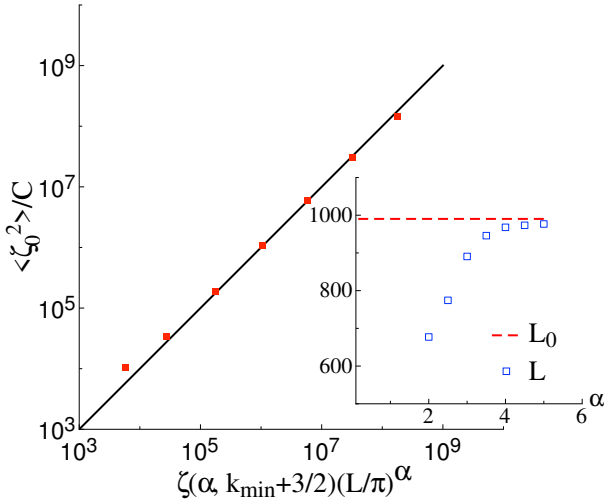

Figure S4: Normalized mean-square amplitudes $\langle\ \zeta_0^2\ \rangle$ as a function of the disorder exponent α and comparison with the analytical expression S12. In the inset we compare the real chain length L_0 to its projection L on the x-axis as a function of α.

S2 Supplementary numerical data

S2.1 Reference state

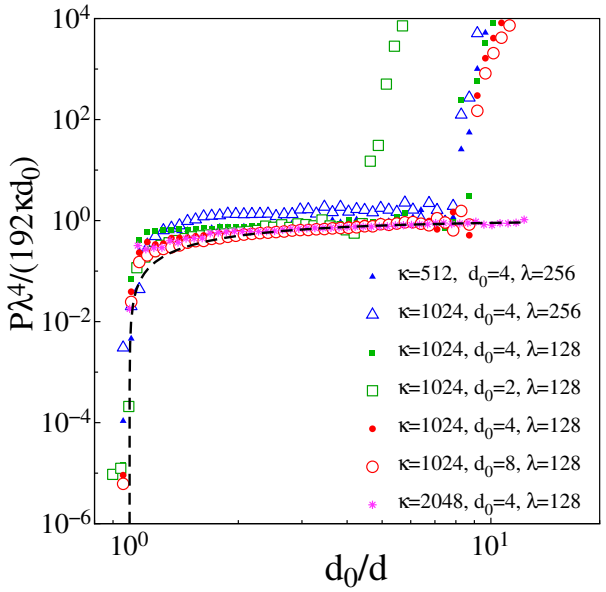

Figure S5: Normalized pressure $P\lambda^4/(192\kappa d_0)$ vs normalized density d_0/d for monomode fiber stacks for various conditions of amplitude ζ_0, bending modulus κ and wavelength λ. The theoretical function $1 - d/d_0$ is also plotted for comparison.

S2.2 Single mode disordered systems

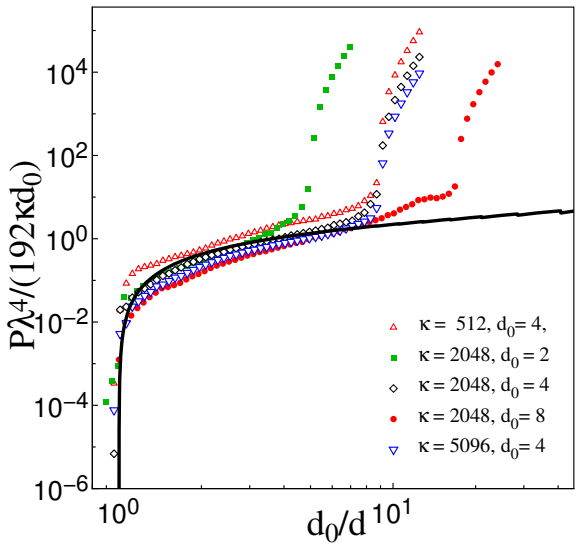

Figure S6: Normalized pressure $P\lambda^4/(192\kappa d_0)$ vs normalized density d_0/d for single mode disordered systems for various conditions of amplitude d_0, bending modulus κ and wavelength λ. The theoretical expression (equation [5] in main text) is also plotted for comparison.

S2.3 Power-law disordered systems and comparison with discrete theory

Fig.S7 display complementary data for comparison between simulations and pressure obtained by solving numerically the self-consistent equation Eq. 2 (main text) for the experimentally determined distributions $\langle \zeta_{0,q}^2 \rangle$.

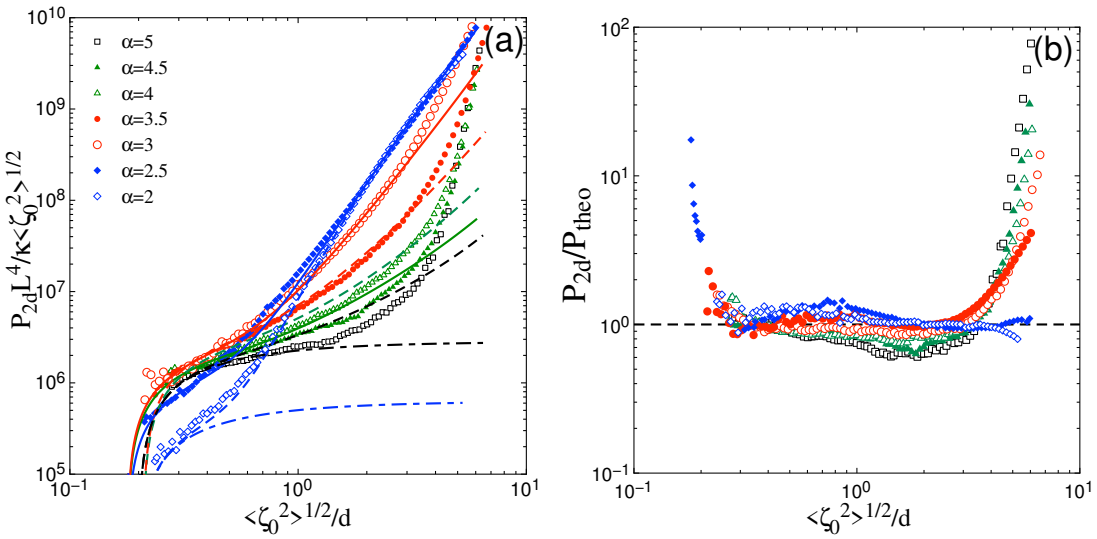

Figure S7: (a) Normalized pressure vs normalized density $\langle \zeta_0^2 \rangle^{1/2}/d$, comparison between numerical simulation data for $\alpha = 2$ to 5 and the sum of the numerical solution of the discrete self-consistent equations (equations 2 and 3 in main text) and the single mode contribution P_{Ref} with wavelength λ corresponding to the first mode of the distribution (dashed-dotted lines P_{Ref} for $\alpha = 2$ and 5). (b) Ratio between numerical simulation pressure and discrete numerical solution of the self-consistent equation. Dashed line corresponds to the scaling solution.

S3 Supplementary theoretical materials

S3.1 Single-mode disorder model (SMD)

For this class of disorder we find numerically that even small perturbations in fiber ordering significantly modify the compression behavior of the fiber stacks in the intermediate compression regime as illustrated by data in Fig. S8.

Results for disordered systems in Fig. S8 suggest that the distribution of wavelengths plays only a minor role in the final compression behaviour that is instead determined by the presence of phase shift randomness. We propose here a simple analytical approach accounting for phase disorder by considering a test fiber with a sinusoidal spontaneous shape of wavelength λ and amplitude d_0. Neighbouring fibers exerce localised forces on the test strand by direct contact, as sketched in Fig. (S8). We compute the deformation of the test fiber by minimizing the bending energy under a prescribed distance d between fibers and a given phase shift measured by x_0, see Fig. S8. By defining the dimensionless variable $u = x_0/\lambda$ and integrating over all the relevant x_0 values we obtain the total pressure P as:

$$\frac{P\lambda^4}{192\kappa d_0} = 2\int_0^{u_{max}} \frac{(1+\cos(2\pi u) - d/d_0)}{(1-2u)^4\,(1+4u)^2} du, \tag{S13}$$

with $2\pi u_{max} = \arccos(d/d_0 - 1)$. Normalised numerical simulations data – see Fig. (S8) – follow a master curve well described by our prediction in Eq. (S13). We also obtained similar results for different fiber

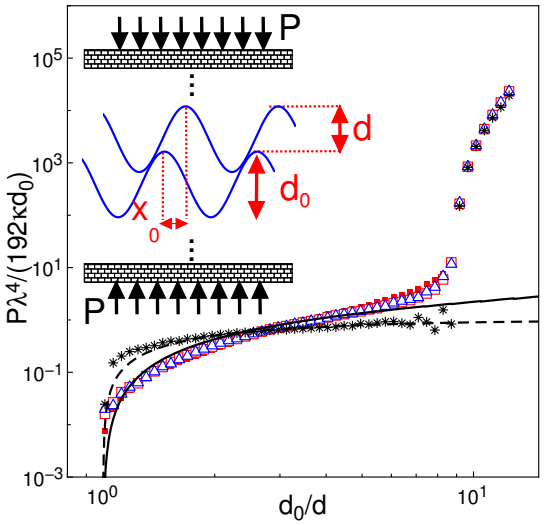

Figure S8: (Color online) Numerical simulation data for normalized pressure $P\lambda^4/(192\kappa d_0)$ *vs* normalized density d_0/d: $(*)$ ordered systems of identical fibers and gaussian disordered systems with variances $\sigma = 0.001$ (□), $\sigma = 0.01$ (■) and $\sigma = 0.1$ (△), see main text. All the simulations presented here have the same bending modulus $\kappa = 2048$, mean wavelength $\lambda = 128$ and amplitude $d_0 = 4$. The dashed line corresponds to the analytical expression P_{Ref} (see main text) and the solid line to equation S13.

systems covering a range of parameters κ, λ and d_0 (see Fig. S6).

S3.2 Self-consistent equation for power-law disordered model (PLD)

S3.2.1 Scaling law analysis

For the disordered shapes described by Eq. S9, using for convenience dimensionless variables $x = d/\sqrt{\langle\zeta_0^2\rangle}$, $\tilde{B} = BL^4/\kappa$ and $\tilde{P} = PL^4/\kappa\sqrt{\langle\zeta_0^2\rangle}$ one gets

$$\langle e\rangle = g(\alpha)\frac{\kappa}{L^4}\frac{\langle\zeta_0^2\rangle}{d}\left(\frac{BL^4}{\kappa}\right)^{(5-\alpha)/4}, \tag{S14}$$

$$\tilde{B}(x) = g(\alpha)\frac{\partial^2}{\partial x^2}\left(\tilde{B}(x)^{(5-\alpha)/4}\right), \tag{S15}$$

$$\tilde{P}(x) = -\int_{x_0}^{x} \mathrm{d}x'\tilde{B}(x'), \tag{S16}$$

with

$$g(\alpha) = -\frac{\pi^{(2\alpha-3)/2}}{2^{(\alpha+1)/2}}\Gamma\left(\frac{7-\alpha}{4}\right)\Gamma\left(\frac{\alpha-5}{4}\right)\zeta\left(\alpha,\frac{5}{2}\right)^{-1}. \tag{S17}$$

Equations S15 and S16 have the scaling solution

$$\tilde{P}_\alpha(d) = c_p(\alpha)\, d^{-\frac{9-\alpha}{\alpha-1}}, \tag{S18}$$

with

$$c_p(\alpha) = \frac{(\alpha-1)}{(9-\alpha)}\left(\frac{2(9-\alpha)(5-\alpha)}{(1-\alpha)^2}g(\alpha)\right)^{4/(\alpha-1)}. \tag{S19}$$

Comparison between the scaling solution Eq. S18 and numerical simulations is shown on Fig. S11 for $\alpha = 2$ to 5 as solid lines using an effective value α_{eff} as a fit parameter. Effective values α_{eff} are

plotted as a function of α on Fig. S12. This again demonstrates the good agreement between numerical simulations and self-consistent theory for $\alpha \sim 2-3$.

S3.2.2 Complete resolution

The complete solution describing also the crossover to zero pressure can be obtained by numerically solving Eqs. S15 and S16. The compression modulus B is given by:

$$B = \frac{\kappa}{L^4}\tilde{B}(x) = g(\alpha)^{4/(\alpha-1)}\frac{\kappa}{L^4}b(x), \tag{S20}$$

where the dimensionless modulus $b(x)$ is solution of the differential equation :

$$b(x) = \frac{\partial^2}{\partial x^2}\left[b(x)^{(5-\alpha)/4}\right]. \tag{S21}$$

As described in the main text, the scaling law $b(x) = b_0 x^{\beta-1}$ with

$$b_0(\alpha) = \left[2\frac{(9-\alpha)(5-\alpha)}{(1-\alpha)^2}\right]^{4/(\alpha-1)} \tag{S22}$$

$$\beta = \frac{9-\alpha}{1-\alpha}. \tag{S23}$$

is a particular solution of the differential Eq. S21.

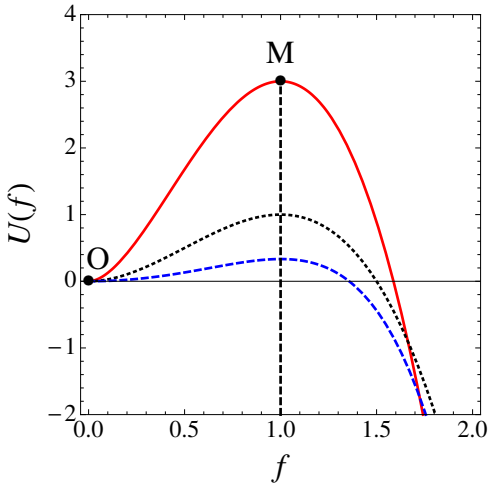

Figure S9: $U(f)$ vs f for $\alpha = 2$ (red solid line), $\alpha = 3$ (black dotted line) and $\alpha = 4$ (blue dashed line).

To find a more general solution of Eq. S21, we define the function $g(x) = b(x)^{(5-\alpha)/4}$ which leads to :

$$g(x)'' = g(x)^{4/(5-\alpha)}. \tag{S24}$$

We look for a general solution of Eq. S24 as $g(x) = g_0 x^p f(x)$ where

$$g_0 = \left[p(\alpha)(p(\alpha)-1)\right]^{(5-\alpha)/(\alpha-1)}, \tag{S25}$$

with $p(\alpha) = 2(5-\alpha)/(1-\alpha)$. Assuming the variable change $x = e^{-t}$ we obtain the following differential equation for f :

$$\ddot{f}(t) = -(1-2p)\dot{f}(t) + p(p-1)\left[f(t)^{1/\gamma} - f(t)\right], \tag{S26}$$

where $\dot{f}$ and $\ddot{f}$ are the first and second derivatives of f with respect to t. This equation is analogous to the one dimensional motion equation of a particle located at f in an external potential $U(f)$, with a fluid friction coefficient $(1-2p)$ (for $\alpha > 1/2$, $(1-2p) < 0$). The external potential $U(f)$ can be expressed as a function of α :

$$U(f) = 2\frac{(5-\alpha)(9-\alpha)}{(1-\alpha)^2}\left[\frac{1}{2}f^2 - \left(\frac{5-\alpha}{9-\alpha}\right)f^{(9-\alpha)/(5-\alpha)}\right], \tag{S27}$$

and has minimum for $f = 0$ and a maximum M at $f = 1$ (see Fig. S9).

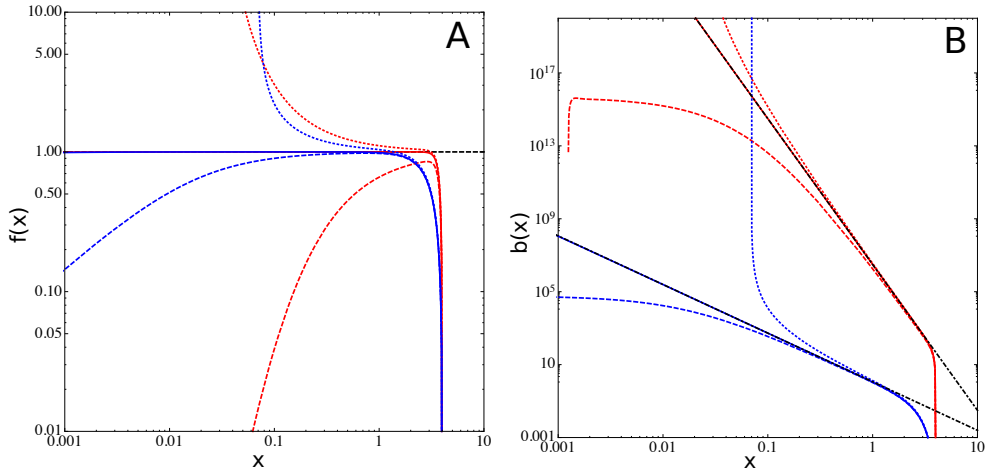

Figure S10: Numerical solution of differential equation S21. (a) $f(x)$ and (b) $b(x)$ for $\alpha = 2$ (red) and $\alpha = 4$ (blue). Solid line for $\dot{f}(t_0) = \dot{f}_c$, dotted line for $\dot{f}(t_0) > \dot{f}_c$ and dashed line for $\dot{f}(t_0) < \dot{f}_c$.

It is now possible to find a solution with a vanishing compression modulus $b(x_c) = 0$ ($f(t_0) = 0$) for $x_c = e^{-t_0}$ (generally $x_c \geq 1 \Leftrightarrow t_0 < 0$). The behavior of $f(t)$ depends on the second boundary condition. We discuss it now in terms of $\dot{f}(t_c)$. We have a particle leaving the point O ($f(t_0) = 0$) (compression modulus $b(x = x_c) = 0$) with an initial velocity $\dot{f}(t_0)$:

- For $\dot{f}(t_0) = \dot{f}_c$ the initial *velocity* of the particle is sufficient to reach the maximum value M for $t \to +\infty$ ($x \to 0$). The particle tends to M and the scaling law $b_0 x^{\beta-1}$ is the asymptotic behavior of the compressibility (see Fig. S10.(a) and S10.(b), solid lines).
- For $\dot{f}(t_0) < \dot{f}_c$ the initial *velocity* of the particle is not large enough to escape from the minimum 0 and to cross the maximum value M. The particle goes close to M and then back to O. The compression modulus is non-monotonic and $b(x) \to 0$ for $x \to 0$ (see Fig. S10.(a) and S10.(b), dashed lines).
- For $\dot{f}(t_0) > \dot{f}_c$ the initial *velocity* of the particle is large enough to escape from the minimum 0 and to cross the maximum value M and the particle leaves the potential well. The compression modulus $b(x) \to +\infty$ for $x \to 0$ (see Fig. S10.(a) and S10.(b), dotted lines).

Figure S11 displays a direct comparison between this complete solution of the self-consistent equation and numerical simulations data, using as fitting parameters x_c and α. The best values of α denoted α_{eff} are represented as a function of α on Fig. S12 confirming again the good agreement between self-consistent theory and numerical simulations for $\alpha \sim 2-3$.

S3.2.3 Comparison with numerical simulations

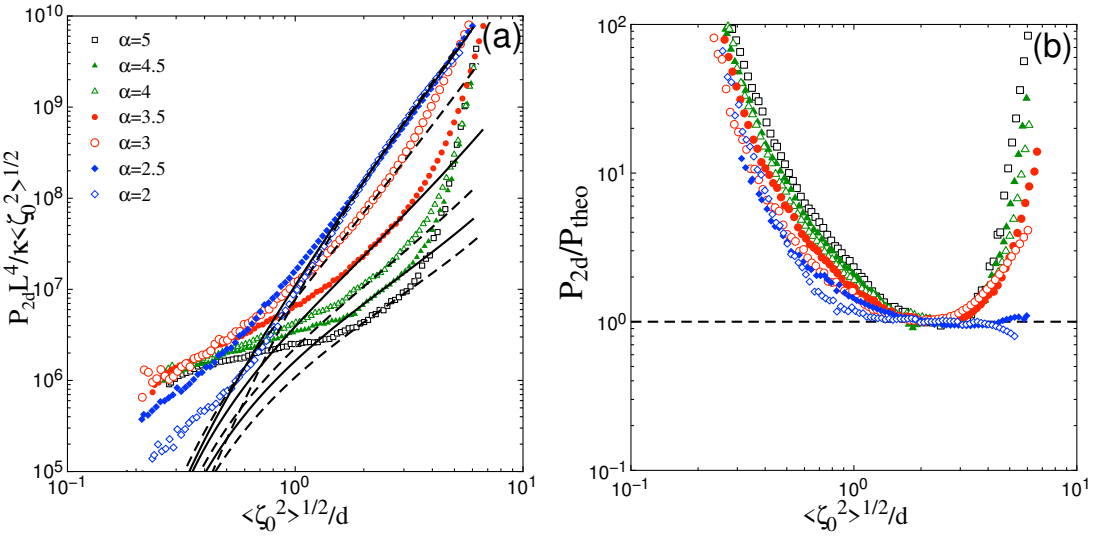

Figure S11: (a) Normalized pressure vs normalized density $\langle\zeta_0^2\rangle^{1/2}/d$, comparison between numerical simulation data for $\alpha = 2$ to 5 and solutions of continuous self-consistent theory with α_{eff} (see Fig. S12), (solid line) scaling law Eq.S18 and (dashed line) complete numerical solution of Eq. S21 using mathematical method described in section S3.2.2 (only for $\alpha = 2, 3, 4$ and 5 for sake of clarity). (b) Numerical simulation pressure and numerical solution of self-consistent equation ratio. Dashed line corresponds to the scaling solution Eq.S18.

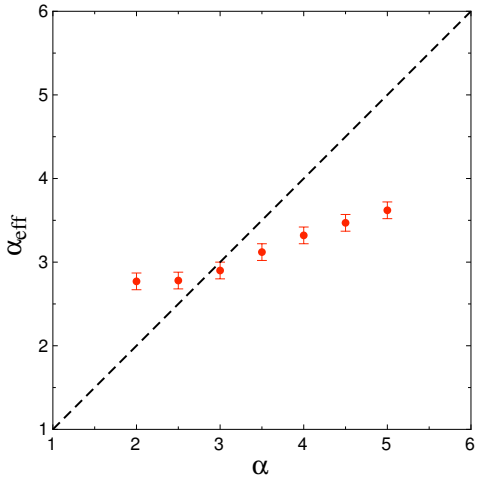

Figure S12: Effective exponent α_{eff} vs α. Dashed line corresponds to $\alpha_{\text{eff}} = \alpha$.

References

[1] A.E.H. Love. *A treatise on the mathematical theory of elasticity*, volume 1. 1892.

[2] L. D. Landau and E. M. Lifshitz. *Theory of Elasticity*. Pergamon Press, New York, 1981.

[3] M. Abramowitz and I. A. Stegun. *Handbook of Mathematical Functions*. Dover, New York, 1964.